Bull. Chem. Soc. Jpn., 71, 867—875 (1998)

Synthesis and Characterization of Ruthenium Terpyridine Dioxolene Complexes: Resonance Equilibrium between Ru^{III}–Catechol and Ru^{II}–Semiquinone Forms

Masato Kurihara,† Stephane Daniele,†† Kiyoshi Tsuge, Hideki Sugimoto, and Koji Tanaka*

Institute for Molecular Science, Myodaiji, Okazaki 444

†Department of Chemistry, School of Science, The University of Tokyo, Hongo, Tokyo 113

††Antipolis Laboratoire de Chimie Moleculaire, Universite de Nice-Sophia, URA CNRS 426, Parc Valrose, 06108 NICE Cedex, France

(Received September 17, 1997)

A series of [RuX(dioxolene)(terpy)] (terpy = terpyridine; X = Cl, OAc) and one-electron oxidized complexes were prepared. The molecular structures of [RuCl($O_2C_6H_2$-3,5-Bu_2)(terpy)] (**1**) and [Ru(OAc)($O_2C_6H_4$)(terpy)] (**3**) were determined by X-ray crystallography. Crystal data for **1**: monoclinic, space group $P2_1/c$, $Z=8$, $a=11.548(1)$, $b=18.224(5)$, $c=30.002(8)$ Å, $\beta=96.51(2)^\circ$, and $R=0.077$ ($R_w=0.068$). Crystal data for **3**: monoclinic, space group $C2/c$, $Z=8$, $a=13.355(5)$, $b=12.131(4)$, $c=26.645(4)$ Å, $\beta=92.46(2)^\circ$, and $R=0.041$ ($R_w=0.041$). Although the binding mode of $O_2C_6H_2$-3,5-Bu_2 to Ru was not determined by the molecular structure of **1**, the carbon–oxygen and carbon–carbon bond lengths of $O_2C_6H_4$ in **3** were consistent with those of catecholato ligands. Electronic absorption spectra of [RuX(dioxolene)(terpy)] were explained by the electronic structure of [Ru^{II}X(semiquinone)(terpy)] rather than [Ru^{III}X(catecholato)(terpy)], while the reverse assignment was deduced from the IR spectra. Moreover, ESR spectra showed hyper-fine structures due to the contribution of semiquinone superimposed on an axial pattern of the Ru(III) center, indicating a resonance equilibrium between [Ru^{II}X(semiquinone)(terpy)] and [RuX(dioxolene)(terpy)].

Polypyridyl-ruthenium(II) complexes are characterized by the ligand localized-redox reactions,[1] which also have been utilized as electron reservoirs in electrochemical reduction of CO_2 catalyzed by those complexes with a good leaving group.[2] The desirable electrocatalysts should have an ability to make energetically unfavorable reactions proceed near the equilibrium potentials with moderate reaction rates. Energy efficiency in those catalytic reactions, therefore, is largely dependent on the redox potentials of metal complexes used as electrocatalysts. The control of ligand localized redox potentials is generally much easier than that of metal-centered ones. Moreover, configurational changes of metal complexes caused by multi-electron transfer to and from ligand localized orbitals usually are not so serious compared with those by multi-electron redox reactions in central metals. Polypyridyl ligands of metal complexes, however, do not work as electron reservoirs in electrocatalysts which operate at potentials more positive than −1.0 V, since polypyridyl metal complexes usually do not undergo ligand localized redox reactions at potentials more positive than −1.0 V (vs. SCE).[3] Accordingly, dioxolene–ruthenium(II) complexes are also feasible electrocatalysts if one considers their characteristics ligand localized redox reactions in a potential range from −0.9 to +1.5 V (vs. Fc/Fc^+).[4] Ruthenium(II) with both dioxolene and polypyridyl ligands, therefore, may become versatile electrocatalysts which can operate in wide potential ranges.

Dioxolene ligands bonded to Ru are expected to serve as two electron reservoirs, because the bonding modes of the ligands to metals are classified to catechol, semiquinone and quinone.[5] Pierpont et al. have prepared a variety of dioxolene metal complexes[6,7] and their physical properties were also examined.[8—10] Although redox reactions of coordinatively saturated ruthenium[11] and osmium complexes[4,12] with bipyridine and dioxolene ligands have been examined, elucidation of redox behavior of Ru(polypyridyl)(dioxolene) complexes with a good leaving substituent is essential to develop a new type of electrocatalysts which can operate in a wide potential range. In this study, we introduced a dioxolene ligand such as 3,5-di-*t*-butylcatecholato, catecholato, tetrachlorocatecholato, and 4-nitrocatecholato into a terpyridine–ruthenium moiety.

Experimental

Materials. [$RuCl_3$(terpy)] (terpy = 2,2′ : 6′,2″-terpyridine) was prepared according to the literature.[13] Special grade catechol (Wako) and extra pure grade 4-nitrocatechol (Tokyo Kasei), 3,5-di-*t*-butylcatechol (Aldrich), and tetrachlorocatechol, 98% (Aldrich) were used as supplied.

Measurements. Electronic absorption spectra were recorded on a Hewlett Packard 8452A diode array spectrophotometer or a

Shimadzu UV-vis-NIR scanning spectrophotometer UV-3100PC. IR spectra were obtained on a Shimadzu FTIR-8100 spectrophotometer. ^{1}H NMR spectra were measured on a JEOL EX270 (270 MHz) spectrometer. ESR spectra were measured on a JEOL JES-FE2XG X-band spectrometer equipped with on Echo Electronics NMR field meter to calibrate the magnetic field and a Takeda Riken microwave counter TR5212 to obtain the microwave frequency, or a Bruker ESR-300E equipped with a Hewlett Packard microwave frequency counter 5352B. Cyclic voltammetric experiments were carried out in a one-compartment cell consisting of a glassy carbon working electrode, a platinum wire auxiliary electrode, and an Ag/Ag^+ reference electrode. A Hokuto Denko HA-151 potentiostat/function generator and Riken Denshi Co. F-35 X–Y recorder were used to collect cyclic voltammetric data. All solutions were deoxygenated by passing a stream of nitrogen gas into the solution at least 10 min prior to recording the data. Ferrocene was added at the end of each experiment as an internal standard: all potentials are quoted vs. the Fc/Fc^+ couple. Spectroelectrochemistry was performed with a thin-layer electrode cell with a platinum mini grid working electrode sandwiched between two glass sides of an optical cell (the path length; 0.5 mm). A platinum wire for an auxiliary electrode and an Ag/Ag^+ reference electrode were separated from the working compartment by a luggin capillary.

Preparation of [RuCl($O_2C_6H_2Bu_2$)(terpy)](1). An ethanol solution (500 μl) of potassium *t*-butoxide (1.38×10^{-4} mol) was injected into an ethanol/chloroform (40 ml), 1 : 1 v/v) solution of 3,5-di-*t*-butylcatechol (16.7 mg, 7.51×10^{-5} mol) with a micro syringe; then the mixture was stirred for 15 min under N_2. Then [$RuCl_3$(terpy)] (30 mg, 6.8×10^{-5} mol) was added into the pale blue solution and the suspension was vigorously stirred at room temperature for 1 d. The resultant purple solution was filtered and the filtrate was evaporated to dryness under reduced pressure. The residue was dissolved into a small amount of ethanol, and purified through a silica-gel column (70—230 mesh). A blue component of Ru–semiquinone complex, [Ru(dbseq)$_3$][9b] first developed with ethanol and then a purple component of **1** eluted with methanol. The collected complex was recrystallized from ethanol/dichloromethane (1 : 1 v/v); yield 17.9 mg (40.2%). Anal. Calcd for $C_{29}H_{31}N_3O_2ClRu\cdot1/2CH_2Cl_2\cdot1/2C_2H_5OH$: C, 55.88; H, 5.38; N, 6.41%. Found: C, 55.91; H, 5.37; N, 6.44%. FAB-mass: 590 ([M]$^+$). IR spectrum (KBr) ν(C–O in catecholato moiety) 1194 cm^{-1}. Electronic spectrum (CH_2Cl_2): 238 (log ε = 4.53), 280 (4.38), 318 (4.40), 370 (3.78), 584 (3.61), and 876 (4.28) nm.

Preparation of [RuCl($O_2C_6H_2Bu_2$)(terpy)]BF_4 (1·BF_4). **1**·1/2CH_2Cl_2·1/2CH_3CH_2OH (100 mg, 1.53×10^{-4} mol) was dissolved into methanol/water (50 ml, 5 : 1 v/v) and 1.1 equiv of $AgBF_4$ was added to oxidize **1**. The solution immediately turned deep blue. After metallic Ag was removed by filtration through a celite layer with suction, the filtrate was reduced in volume under the reduced pressure below 25 °C to give an blue precipitate of **1**·BF_4, which was collected by filtration; yield 98.0 mg (94.9%). Anal. Calcd for $C_{29}H_{31}BClF_4N_3O_2Ru$: C, 51.46; H, 4.62; N, 6.21%. Found: C, 51.64; H, 4.53; N, 6.24%. FAB-mass: 590 ([M] – BF_4). IR spectrum (KBr) ν(C=O in the quinone moiety) 1601 cm^{-1}. Electronic spectrum (acetone): 212 (log ε = 4.30), 328 (4.16), and 592 (4.19) nm. ^{1}H NMR (CD_3CN, R.T.) δ = 1.11 (9H, s, *t*-Bu), 1.31 (9H, s, *t*-Bu), 1.44 (9H, s, *t*-Bu), 1.74 (9H, s, *t*-Bu), 8.54 and 8.57 (2H, d, *J* = 8.3 Hz, terpy), 8.52 and 8.55 (2H, d, *J* = 8.3 Hz, terpy), 8.33 and 8.36 (4H, d, *J* = 8.3 Hz, terpy), 7.9—8.1 (3H, t, t, terpy), 7.44 (2H, t, *J* = 6.8 Hz, terpy), 7.22 (2H, d, *J* = 5.9 Hz, terpy), 8 and 7.24 (4H, s, dbq). The four signals of *t*-Bu groups of dbqui derived from 1 : 1 two geometrical isomers.

Preparation of [Ru(OAc)($O_2C_6H_2Bu_2$)(terpy)] (2). Into a methanol solution (100 ml) of 3,5-di-*t*-butylcatechol (101 mg, 4.54×10^{-4} mol), [$RuCl_3$(terpy)] (200 mg, 4.54×10^{-4} mol) was added; then the suspension was stirred for 30 min under N_2. Then, an excess amount of potassium acetate (400 mg, 4.08×10^{-3} mol) was added into the suspension and the mixture was vigorously stirred for 2 d at room temperature. The resulting purple solution was evaporated under reduced pressure and the residue was extracted with acetone to remove excess amount of potassium acetate. The acetone solution was loaded on a silica-gel column. After [Ru(dbseq)$_3$][9b] and **1** eluted with acetone, [Ru(OAc)(dbcat)(terpy)] adsorbed on the top of the column was eluted with methanol and the crude product was recrystallized from methanol–water (5 : 1 v/v); yield 150 mg (51.6%). Anal. Calcd for $C_{31}H_{34}N_3O_4Ru\cdot3/2H_2O$: C, 58.11; H, 5.82; N, 6.56%. Found: C, 58.27; H, 5.74; N, 6.52%. FAB-mass: 614 ([M]$^+$). IR spectrum (KBr) ν(C–O in the catecholato moiety) 1198 and ν_{as}(C=O in OAc) 1578 and ν_s (C=O in OAc) 1325 cm^{-1}. Electronic spectrum (CH_2Cl_2): 214 (log ε = 4.61), 280 (4.39), 317 (4.38), 370 (3.73), 576 (3.52), and 883 (4.27) nm. The number of molecules of water as the crystal solvent was confirmed by ^{1}H NMR integral ratio in acetone-d_6.

Preparation of [Ru(OAc)($O_2C_6H_2Bu_2$)(terpy)]PF_6 (2·PF_6). A purple methanol–water (5 : 1 v/v) solution (50 ml) of [Ru(OAc)($O_2C_6H_2Bu_2$)(terpy)]·3/2H_2O (200 mg, mol) was immediately turned to deep blue by an addition of 1.1 equiv of $AgPF_6$. After the solution was filtered through a celite layer with suction, the deep blue solution was reduced in volume under reduced pressure below 25 °C to give a blue precipitate of [Ru(OAc)($O_2C_6H_2Bu_2$)(terpy)]-PF_6, which was collected by filtration and recrystallized from acetone/toluene (1 : 1 v/v); yield 235 mg (96.3%). Anal. Calcd for $C_{31}H_{34}F_6N_3O_4PRu\cdot1/4C_7H_8$: C, 50.32; H, 4.64; N, 5.34%. Found: C, 49.92; H, 4.63; N, 5.24%. FAB-mass: 614 ([M] – PF_6). IR spectrum (KBr) ν(C=O in the quinone moiety) 1603 and ν_{as}(C=O in OAc) 1632 and ν_s(C=O in OAc) 1304 cm^{-1}. Electronic spectrum (acetone): 214 (log ε = 4.34), 326 (4.20), and 584 (4.23) nm. ^{1}H NMR (acetone-d_6, R.T.) δ = 1.17 (4.5H, s, *t*-Bu), 1.45 (4.5H, s, *t*-Bu), 1.27 (9H, s, *t*-Bu), 1.73 (9H, s, *t*-Bu), 8.76 and 8.79 (2H, d, *J* = 7.9 Hz, terpy), 8.74 and 8.77 (1H, d, *J* = 8.2 Hz, terpy), 8.61 and 8.58 (2H, d, *J* = 8.2 Hz, terpy), 8.6 and 8.56 (1H, d, terpy), 8.14 (3H, t, *J* = 8.6 Hz, terpy), 8.05 (1.5H, t, terpy), 7.55 (3H, dd, terpy), 7.38 (3H, d, terpy), 8.08 and 7.31 (3H, s and d, dbq), 2.17 (4.5H, s, OAc). The four signals of *t*-Bu groups of dbqui derived from 2 : 1 two geometrical isomers. The numbers of molecules of toluene as the crystal solvent was confirmed by ^{1}H NMR integral ratio.

Preparation of [Ru(OAc)($O_2C_6H_4$)(terpy)] (3). This complex was prepared similarly to **2** by using catechol in place of 3,5-di-*t*-butylcatechol; it was recrystallized from methanol/water (5 : 1 v/v); yield 58.5%. Anal. Calcd for $C_{23}H_{18}N_3O_4Ru\cdot3/2H_2O$: C, 52.27; H, 4.01; N, 7.95%. Found: C, 52.15; H, 3.76; N, 7.96%. FAB-mass: 502 ([M]$^+$). IR spectrum (KBr) ν(C–O in the catechol moiety) 1240 and ν_{as}(C=O in OAc) 1595 and ν_s(C=O in OAc) 1314 cm^{-1}. Electronic spectrum (dichloromethane) 225 (log ε = 4.50), 279 (4.38), 316 (4.36), 371 (3.73), 534 (3.54), and 878 (4.18)-nm. The number of molecules of water as the crystal solvent was confirmed by ^{1}H NMR integral ratio in methanol-d_4.

Preparation of [Ru(OAc)($O_2C_6H_4$)(terpy)]PF_6 (3·PF_6). The oxidation of **3** with $AgPF_6$ was conducted under the same procedure as for the transformation from **2** to **2**$^+$; yield 95.2%. Anal. Calcd for $C_{23}H_{18}N_3O_4Ru\cdot C_3H_6O$: C, 44.33; H, 3.43; N, 5.96%. Found: C, 44.97; H, 3.14; N,6.10%. FAB-mass: 502 ([M]–PF_6). IR spectrum (KBr) ν(C–O in the quinone moiety) 1605 and ν_{as}(C=O in OAc) 1622 and ν_s(C=O in OAc) 1318 cm^{-1}. Electronic spectrum (ace-

tone): 212 (log ε = 4.30), 324 (4.17), and 556 (4.15) nm. ^{1}H NMR (acetone-d_6, R.T.) δ = 8.76 and 8.79 (2H, d, J = 8.3 Hz, terpy), 8.52 and 8.55 (2H, d, J = 8.3 Hz, terpy), 8.10 (2H, td, J = 7.9 and 1.7 Hz, terpy), 7.95 (1H, t, J = 8.1 Hz, terpy), 7.52 (2H, dd, J = 13.2 and 6.6 Hz, terpy), 7.22 and 7.25 (2H, d, J = 8.2 Hz, terpy), for bqui ligand 8.41 and 8.44 (1H, d, J = 8.6 Hz), 7.44 and 7.47 (1H, d, J = 8.6 Hz), 7.13—7.22 (2H, m), for OAc ligand 2.31 (3H, s).

Preparation of [Ru(OAc)($Cl_4O_2C_6H_4$)(terpy)] (4). Into a methanol solution (100 ml) of tetrachlorocatechol (172 mg, 6.94×10^{-4} mol), [$RuCl_3$(terpy)] (307 mg, 6.97×10^{-4} mol) was added; then the suspension was stirred for 30 min under N_2. An excess amount of potassium acetate (550 mg, 5.60×10^{-3} mol) was added to the suspension and the mixture was stirred for 30 h at room temperature. The solvent was removed under reduced pressure to dryness and the excess of potassium salt was eliminated by washing with a minimum amount of cold water. After the resulting black precipitate was further washed with Et_2O, the crude product was dissolved in acetone, and then loaded on a silica-gel column. After the chloride analogue was eluted with acetone, [Ru(OAc)-($O_2C_6Cl_4$)(terpy)] adsorbed on the top of the column was eluted with methanol. The solvent was removed and the complex **4** was recrystallized from methanol; yield 102 mg (21.0%). Anal. Calcd for $C_{23}H_{14}Cl_4N_3O_4Ru\cdot3H_2O$: C, 39.77; H, 2.88; N, 6.05%. Found: C, 40.04; H, 2.33; N, 5.98%. FAB-mass: 640 ([M]$^+$). IR spectrum (KBr) ν(C–O in the catecholato moiety) 1256 and ν_{as}(C=O in OAc) 1611 and ν_s(C=O in OAc) 1318 cm^{-1}. Electronic spectrum (dichloromethane): 226 (log ε = 4.70), 277 (4.41), 315 (4.39), 511 (3.51), 849 (4.06), and 884 (4.07) nm.

Preparation of [Ru(OAc)($O_2C_6H_3NO_2$)(terpy)] (5). This complex was prepared similarly to **4** by using 4-nitrocatechol (140 mg, 9.03×10^{-4} mol) in place of tetrachlorocatechol; yield 245 mg (46.7%). Anal. Calcd for $C_{23}H_{17}N_4O_6Ru\cdot2H_2O$: C, 47.36; H, 3.60; N, 9.61%. Found: C, 47.99; H, 3.26; N, 9.68%. FAB-mass: 547 ([M]$^+$). IR spectrum (KBr) ν(C–O in the catecholato moiety) 1283 and 1273 and ν_{as}(C=O in OAc)1588 and ν_s(C=O in OAc) 1318 cm^{-1}. Electronic spectrum (dichloromethane): 225 (log ε = 4.43), 277 (4.31), 317 (4.29), 371 (3.88), 506 (3.64), 829 (3.92), and 855 (3.91) nm. The number of molecules of water as the crystal solvent in complexes **4** and **5** was confirmed by ^{1}H NMR integral ratio in acetone-d_6.

X-Ray Crystallographic Study. Single crystals of **1** were obtained by recrystallization from ethanol/dichloromethane (1 : 1 v/v) under slow evaporation of dichloromethane at room temperature. Single crystals of **3** were grown from a methanol/water solution. The crystals were mounted on glass capillaries. X-Ray measurements were performed on an Enraf Nonius CAD4-GX21 diffractometer for **1** and a Rigaku AFC-5S diffractometer for **3**. The crystallographic data are presented in Table 1. The radiation used was Mo $K\alpha$ monochromated with a graphite monochrometer. The intensities of the reflections of the two crystals did not decay, and the data were corrected for the *Lp* factor and empirically for the absorption.

All the calculations were performed with the teXsan crystallographic software package.[14] The positions of ruthenium atoms were determined by the direct method,[15] and other non-hydrogen atoms were located in successive Fourier maps for **1**. There were two independent molecules in a unit cell of **1**. Two ruthenium atoms and the atoms ligating to the ruthenium atoms were refined anisotropically and other non-hydrogen atoms were refined isotropically. The hydrogen atoms were fixed at the calculated positions. The structure was refined with full-matrix least-square techniques. Selected atomic positional parameters for **1** are given in Table 2.

Table 1. Crystal Parameters and X-Ray Diffraction Data for **1**·1/2CH_2Cl_2·1/2C_2H_5OH and **3**·3/2H_2O

	1·1/2CH_2Cl_2·1/2C_2H_5OH	**3**·3/2H_2O
Formula	$C_{30.5}H_{35}Cl_2O_{2.5}N_3Ru$	$C_{23}H_{20.5}O_{2.5}N_3Ru$
FW	655.6	528.5
Space group	$P2_1/c$	$C2/c$
a/Å	11.548(1)	13.355(5)
b/Å	18.224(5)	12.131(4)
c/Å	30.002(8)	26.645(4)
β/deg	96.51(2)	92.46(2)
V/Å^3	6273(3)	4312(1)
Z	8	8
T/K	293	293
ρ_{calc}/gcm^{-3}	1.39	1.63
μ/cm^{-1}	7.02	7.71
GOF	1.96	1.45
R[a]	0.077	0.041
R_w[b]	0.068	0.041

a) $R=\sum||F_o|-|F_c||/\sum|F_o|$.
b) $R_w=[(\sum w(|F_o|-|F_c|)^2/\sum w(F_o)^2)]^{1/2}$.

In the Fourier map, one dichloromethane and one ethanol molecules were found as the crystal solvents. The atomic parameters of these molecules did not converge to reasonable values with the occupation factors, 1.0. We changed the occupation factors of these molecules and the atomic parameters converged with occupation factors 0.5. The elemental analysis also showed good agreement with the formula:[Ru(terpy)($O_2C_6H_2Bu_2$)-Cl]·1/2CH_2Cl_2·1/2C_2H_5OH.

The structure of **3** was solved by heavy-atom methods and expanded using Fourier techniques. The positional and thermal parameters of non-hydrogen atoms were refined anisotropically by the full-matrix least-squares method. The positions of hydrogen atoms except for water molecules were refined by full-matrix least-squares method and other parameters of hydrogen atoms were not refined. Selected atomic positional parameters for **3** are given in Table 3.

Lists of detailed crystallographic data, calculated positional parameters, anisotropic thermal parameters, complete bond lengths and angles are deposited as Document No. 71017 at the Office of the Editor of Bull. Chem. Soc. Jpn.

Results and Discussion

Syntheses. It has been reported that the reaction of [$RuCl_3$(terpy)] with 3,5-di-*t*-butylcatechol in the presence of NEt_3 produces [RuCl($O_2C_6H_2Bu_2$)(terpy)] (**1**) in EtOH.[16] The same neutral complex (**1**) was also prepared by the reaction of [$RuCl_3$(terpy)] with a stoichiometric amount of 3,5-di-*t*-butylcatechol in the presence of *t*-BuOK in EtOH/$CHCl_3$, and the acetato derivative, [Ru-(OAc)($O_2C_6H_2Bu_2$)(terpy)], (**2**) was obtained by the reaction of [$RuCl_3$(terpy)] with 3,5-di-*t*-butylcatechol in the presence of a large excess of CH_3COOK. Similarly, the reactions of [$RuCl_3$(terpy)] with $C_6H_4(OH)_2$, $C_6Cl_4(OH)_2$, and 4-$NO_2C_6H_3(OH)_2$ in the presence of a large excess of CH_3COOK gave [Ru(OAc)($O_2C_6H_4$)(terpy)] (**3**), [Ru-(OAc)($O_2C_6Cl_4$)(terpy)] (**4**), and [Ru(OAc)($O_2C_6H_3NO_2$)-(terpy)] (**5**), respectively. Treatments of **1** and **2** with $AgBF_4$ gave cationic [RuCl($O_2C_6H_2Bu_2$)(terpy)]BF_4 (**1**·BF_4) and [Ru(OAc)($O_2C_6H_2Bu_2$)(terpy)]BF_4 (**2**·BF_4), respectively.

Table 2. Atomic Parameters for $\mathbf{1}\cdot 1/2CH_2Cl_2\cdot 1/2C_2H_5OH$

Atom	x	y	z	$B_{eq}/Å^2$	Atom	x	y	z	$B_{eq}/Å^2$
Ru1	0.7733(2)	0.1285(1)	0.03082(6)	3.30(5)	C23	0.806(2)	−0.073(1)	−0.0319(7)	5.0(6)
Ru2	0.2392(2)	0.39522(10)	−0.05093(6)	3.36(5)	C24	0.816(2)	0.000(1)	−0.0167(7)	3.3(5)
Cl1	0.6424(5)	0.1682(3)	−0.0321(2)	4.3(2)	C25	0.902(2)	0.054(1)	−0.0310(7)	3.1(5)
Cl2	0.1449(5)	0.3199(3)	−0.0004(2)	4.8(2)	C26	0.984(2)	0.041(1)	−0.0624(7)	3.8(5)
Cl3	0.799(2)	0.249(1)	0.3516(7)	15.3(7)	C27	1.050(2)	0.095(1)	−0.0763(7)	4.4(6)
Cl4	0.699(2)	0.374(1)	0.3417(7)	14.8(7)	C28	1.042(2)	0.161(1)	−0.0567(7)	5.0(6)
O1	0.878(1)	0.1089(7)	0.0878(4)	3.9(4)	C29	0.965(2)	0.174(1)	−0.0239(7)	4.2(6)
O2	0.802(1)	0.2322(7)	0.0544(4)	3.9(4)	C30	0.353(2)	0.405(1)	−0.1277(7)	3.4(5)
O3	0.324(1)	0.4463(7)	−0.0942(5)	4.2(4)	C31	0.311(2)	0.332(1)	−0.1275(7)	2.7(5)
O4	0.255(1)	0.3100(8)	−0.0965(4)	3.8(4)	C32	0.333(2)	0.285(1)	−0.1626(7)	3.4(5)
O5	0.200(3)	0.244(2)	0.124(1)	7.4(10)	C33	0.399(2)	0.316(1)	−0.1943(7)	4.3(6)
N1	0.637(2)	0.0971(9)	0.0645(5)	3.8(5)	C34	0.443(2)	0.391(1)	−0.1937(7)	4.1(5)
N2	0.755(1)	0.0266(8)	0.0123(5)	2.2(4)	C35	0.416(2)	0.434(1)	−0.1614(7)	3.7(5)
N3	0.898(1)	0.1195(9)	−0.0117(5)	3.5(5)	C36	0.288(2)	0.207(1)	−0.1671(7)	3.3(5)
N4	0.085(1)	0.4374(9)	−0.0779(5)	3.6(5)	C37	0.315(2)	0.166(1)	−0.2083(9)	8.5(8)
N5	0.230(1)	0.4793(8)	−0.0152(5)	1.7(4)	C38	0.160(2)	0.209(1)	−0.1697(8)	6.9(7)
N6	0.385(1)	0.3827(9)	−0.0087(5)	3.5(5)	C39	0.334(2)	0.166(1)	−0.1258(8)	5.9(7)
C1	0.878(2)	0.166(1)	0.1153(7)	3.3(5)	C40	0.509(3)	0.417(2)	−0.2303(9)	8.6(8)
C2	0.835(2)	0.233(1)	0.0971(7)	3.1(5)	C41	0.564(3)	0.366(2)	−0.256(1)	17(1)
C3	0.843(2)	0.301(1)	0.1197(7)	3.9(6)	C42	0.439(3)	0.462(2)	−0.261(1)	16(1)
C4	0.879(2)	0.297(1)	0.1629(7)	4.1(6)	C43	0.609(3)	0.461(2)	−0.211(1)	16(1)
C5	0.915(2)	0.231(1)	0.1849(7)	4.6(6)	C44	0.014(2)	0.411(1)	−0.1107(7)	4.0(6)
C6	0.916(2)	0.166(1)	0.1627(7)	3.1(5)	C45	−0.096(2)	0.444(1)	−0.1279(8)	6.8(7)
C7	0.879(2)	0.366(2)	0.1977(9)	8.0(8)	C46	−0.126(2)	0.506(1)	−0.1115(8)	6.8(7)
C8	0.840(2)	0.433(2)	0.1719(9)	8.2(8)	C47	−0.046(2)	0.538(1)	−0.0759(8)	6.3(7)
C9	0.814(4)	0.353(3)	0.230(2)	21(1)	C48	0.059(2)	0.505(1)	−0.0583(7)	4.3(6)
C10	1.009(3)	0.382(2)	0.215(1)	16(1)	C49	0.146(2)	0.527(1)	−0.0246(7)	3.7(6)
C11	0.961(2)	0.092(2)	0.1860(9)	8.3(8)	C50	0.139(2)	0.597(1)	−0.0028(7)	4.7(6)
C12	0.859(3)	0.037(2)	0.1785(10)	9.7(9)	C51	0.231(2)	0.612(1)	0.0311(7)	6.0(7)
C13	0.970(2)	0.102(2)	0.2388(10)	10.6(9)	C52	0.318(2)	0.561(1)	0.0406(7)	4.8(6)
C14	1.066(3)	0.067(2)	0.1728(10)	9.7(9)	C53	0.319(2)	0.498(1)	0.0168(7)	3.8(6)
C15	0.584(2)	0.139(1)	0.0928(7)	4.6(6)	C54	0.406(2)	0.437(1)	0.0230(7)	3.3(5)
C16	0.492(2)	0.111(1)	0.1148(7)	5.4(6)	C55	0.499(2)	0.436(1)	0.0564(7)	3.8(6)
C17	0.452(2)	0.040(1)	0.1063(8)	6.4(7)	C56	0.570(2)	0.375(1)	0.0593(7)	5.0(6)
C18	0.513(2)	−0.001(1)	0.0765(7)	3.5(5)	C57	0.556(2)	0.323(1)	0.0284(8)	5.9(7)
C19	0.600(2)	0.025(1)	0.0574(7)	3.1(5)	C58	0.465(2)	0.327(1)	−0.0046(7)	3.8(6)
C20	0.669(2)	−0.013(1)	0.0265(7)	2.8(5)	C59	0.356(3)	0.319(2)	0.153(1)	3(1)
C21	0.650(2)	−0.085(1)	0.0159(7)	4.4(6)	C60	0.269(5)	0.292(4)	0.116(2)	10(1)
C22	0.721(2)	−0.114(1)	−0.0144(6)	4.3(6)	C61	0.701(5)	0.287(3)	0.356(2)	8(1)

Complex **3** was also easily oxidized by $AgPF_6$ to give [Ru(OAc)($O_2C_6H_4$)(terpy)](PF_6) (**3**·PF_6). On the other hand, **4** and **5** having strong electron-withdrawing substituents were not oxidized by $AgBF_4$ because of a substantial positive shift of their redox potentials (vide infra).

Crystal structure. The crystal structure of **1** is depicted in Fig. 1. There are two isomers resulting from the difference in the positions of two *t*-Bu groups in the C_6 ring. The two isomers are stacked separately with a dimer unit. Three nitrogen atoms of terpyridine and one oxygen atom of $O_2C_6H_2Bu_2$ form the equatorial plane, and the remaining oxygen atom of the ligand and Cl are linked to Ru in the axial positions. Bulky $O_2C_6H_2Bu_2$ are located in the column to minimize disorder of overlapping of the terpyridine planes,[17] which are separated by a distance in the range of 3.2 to 3.5 Å (Fig. 2). The isomer's columns were well loaded alternately in the *ac*-plane with inclusion of dichloromethane and ethanol as the crystal solvent in a unit cell. Intramolecular bond distances and angles are listed in Table 4. The crystal structure of **3** is shown in Fig. 3. The molecular structures of **1** and **3** are similar to each other. Intramolecular bond distances and

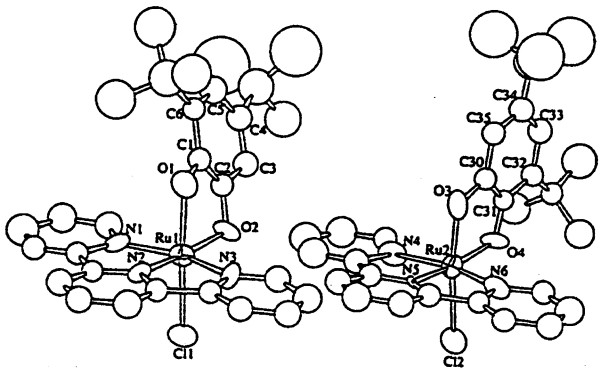

Fig. 1. Molecular structures of the two isomers of [RuCl(dbcat)(terpy)].

Table 3. Atomic Parameters for $3 \cdot 3/2H_2O$

Atom	x	y	z	$B_{eq}/Å^2$
Ru1	−0.33027(4)	0.13087(4)	−0.13193(2)	3.30(1)
O1	−0.3976(3)	−0.0173(3)	−0.1364(1)	3.8(1)
O2	−0.2232(3)	0.0428(3)	−0.0936(1)	3.8(1)
O3	−0.4558(3)	0.1851(3)	−0.1726(1)	4.2(1)
O4	−0.4514(4)	0.3635(4)	−0.1539(2)	6.6(1)
O5	−0.5000	0.0114(5)	−0.2500	5.0(2)
O6	−0.5255(3)	0.5652(4)	−0.1289(2)	6.1(1)
N1	−0.3848(3)	0.1901(4)	−0.0665(2)	3.7(1)
N2	−0.2574(3)	0.2700(4)	−0.1250(2)	3.6(1)
N3	−0.2495(3)	0.1286(4)	−0.1963(2)	3.7(1)
C1	−0.3419(4)	−0.0948(5)	−0.1134(2)	3.5(2)
C2	−0.3734(5)	−0.2052(5)	−0.1121(2)	4.4(2)
C3	−0.3134(6)	−0.2820(6)	−0.0878(3)	5.4(2)
C4	−0.2234(6)	−0.2507(6)	−0.0654(3)	5.7(2)
C5	−0.1904(5)	−0.1429(6)	−0.0660(3)	4.7(2)
C6	−0.2495(4)	−0.0629(5)	−0.0906(2)	3.5(1)
C7	−0.4533(5)	0.1429(6)	−0.0379(2)	4.5(2)
C8	−0.4845(6)	0.1873(7)	0.0056(3)	5.5(2)
C9	−0.4453(6)	0.2859(7)	0.0213(3)	6.2(2)
C10	−0.3748(6)	0.3378(6)	−0.0068(3)	5.4(2)
C11	−0.3459(4)	0.2887(5)	−0.0510(2)	4.1(2)
C12	−0.2724(5)	0.3347(5)	−0.0843(2)	3.9(1)
C13	−0.2203(6)	0.4333(6)	−0.0791(3)	5.2(2)
C14	−0.1545(6)	0.4637(6)	−0.1152(4)	6.0(2)
C15	−0.1403(5)	0.3978(6)	−0.1565(3)	5.0(2)
C16	−0.1933(4)	0.2987(5)	−0.1610(2)	4.0(2)
C17	−0.1900(4)	0.2176(5)	−0.2016(2)	3.9(1)
C18	−0.1295(5)	0.2279(6)	−0.2421(3)	5.2(2)
C19	−0.1241(5)	0.1436(7)	−0.2756(3)	5.5(2)
C20	−0.1824(6)	0.0519(7)	−0.2701(3)	5.5(2)
C21	−0.2462(5)	0.0471(6)	−0.2301(3)	4.5(2)
C22	−0.4925(5)	0.2795(6)	−0.1729(2)	4.5(2)
C23	−0.5950(6)	0.2923(7)	−0.1979(3)	6.0(2)
H1	−0.438(4)	−0.225(5)	−0.129(2)	5.9
H2	−0.336(5)	−0.354(5)	−0.087(2)	5.9
H3	−0.190(5)	−0.293(5)	−0.049(2)	5.9
H4	−0.131(4)	−0.116(5)	−0.052(2)	5.9
H5	−0.476(5)	0.075(5)	−0.050(2)	5.9
H6	−0.537(4)	0.150(5)	0.021(2)	5.9
H7	−0.463(4)	0.322(5)	0.053(2)	5.9
H8	−0.345(4)	0.402(5)	0.004(2)	5.9
H9	−0.229(5)	0.473(5)	−0.053(2)	5.9
H10	−0.113(5)	0.516(5)	−0.113(2)	5.9
H11	−0.082(4)	0.419(5)	−0.183(2)	5.9
H12	−0.097(4)	0.295(5)	−0.245(2)	5.9
H13	−0.080(4)	0.150(5)	−0.301(2)	5.9
H14	−0.176(5)	−0.011(5)	−0.291(2)	5.9
H15	−0.293(4)	−0.011(5)	−0.226(2)	5.9
H16	−0.612(5)	0.232(5)	−0.221(2)	5.9
H17	−0.638(5)	0.260(5)	−0.177(2)	5.9
H18	−0.606(4)	0.373(5)	−0.201(2)	5.9

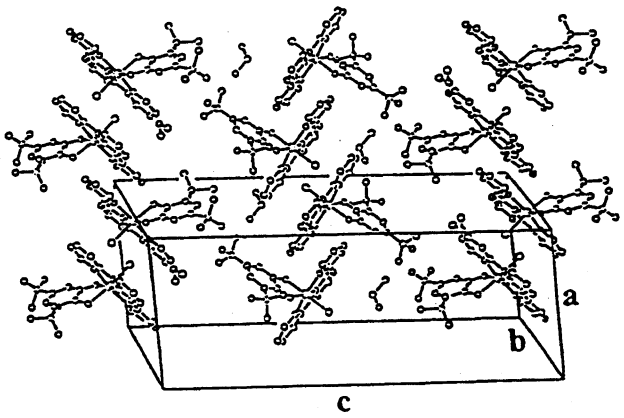

Fig. 2. Packing diagram of the complex **1** viewed down the **b**-axis.

Table 4. Selected Interatomic Distances and Bond Angles in $1 \cdot 1/2CH_2Cl_2 \cdot 1/2C_2H_5OH$

	Interatomic distances (Å)		
Ru1–Cl1	2.393(6)	Ru2–Cl2	2.396(6)
Ru1–O1	2.01(1)	Ru2–O3	1.95(1)
Ru1–O2	2.03(1)	Ru2–O4	2.09(1)
Ru1–N1	2.04(2)	Ru2–N4	2.02(2)
Ru1–N2	1.94(1)	Ru2–N5	1.88(1)
Ru1–N3	2.04(2)	Ru2–N6	2.00(2)
O1–C1	1.33(2)	O3–C30	1.33(2)
O2–C2	1.30(2)	O4–C31	1.26(2)
C1–C2	1.41(3)	C30–C31	1.41(2)
C2–C3	1.41(3)	C31–C32	1.41(2)
C3–C4	1.32(3)	C32–C33	1.40(3)
C4–C5	1.41(3)	C33–C34	1.46(3)
C5–C6	1.35(3)	C34–C35	1.31(3)
C1–C6	1.44(2)	C30–C35	1.42(3)
	Bond angles (deg)		
Cl1–Ru1–O1	171.7(4)	Cl2–Ru2–O3	173.5(4)
Cl1–Ru1–O2	93.2(4)	Cl2–Ru2–O4	93.8(4)
O1–Ru1–O2	79.1(5)	O3–Ru2–O4	80.4(5)
N1–Ru1–N2	78.9(7)	N4–Ru2–N5	79.2(6)
N2–Ru1–N3	79.0(7)	N5–Ru2–N6	80.2(6)
N1–Ru1–N3	157.8(6)	N4–Ru2–N6	159.3(6)
Ru1–O1–C1	110(1)	Ru2–O3–C30	114(1)
Ru1–O2–C2	112(1)	Ru2–O4–C31	109(1)
O1–Ru1–N1	87.2(6)	O3–Ru2–N4	92.0(6)
O1–Ru1–N2	96.4(6)	O3–Ru2–N5	93.2(6)
O1–Ru1–N3	96.8(6)	O3–Ru2–N6	91.6(6)
O2–Ru1–N1	101.0(6)	O4–Ru2–N4	99.1(6)
O2–Ru1–N2	175.5(6)	O4–Ru2–N5	173.4(6)
O2–Ru1–N3	101.2(6)	O4–Ru2–N6	101.6(6)

angles of **3** are listed in Table 5. The acetato ligand in **3** takes the place of the Cl ligand in **1**, namely, the acetato ligand coordinates in monodentate form at axial position against terpyridine plane. The non-coordinate oxygen atom of the acetato ligand is located on the terpyridine side rather than the chelating ligand side. In the crystal structure of **3** there are two kinds of water molecules as crystal solvent. These water molecules interact with oxygen atoms of acetato and dioxolene ligands by a hydrogen bond to form a hydrogen bond network. The water oxygen atom O(6) interacts with acetato oxygen atom O(4) (2.733(7) Å) and dioxolene oxygen atom O(2) (2.852(6) Å). Another water oxygen atom O(5) interacts with acetato oxygen atom O(3) (2.990(6) Å).

The dioxolene complexes of **1**—**5** are expected to have formally three resonance isomers of Eq. 1, where qui, seq, and cat denote quinone, semiquinone and catechol forms,

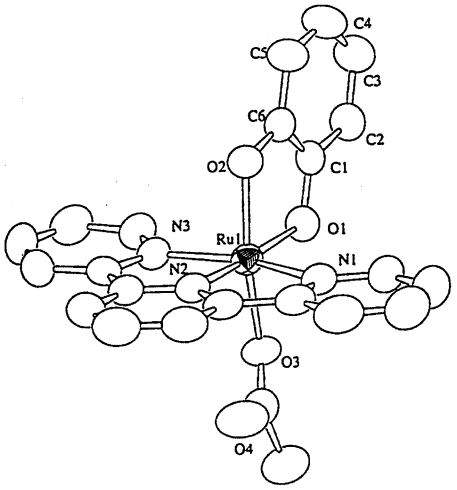

Fig. 3. Molecular structure of [Ru(OAc)(cat)(terpy)].

Table 5. Selected Interatomic Distances and Bond Angles in $3 \cdot 3/2H_2O$

	Interatomic distances (Å)		
Ru(1)–O(1)	2.011(4)	Ru(1)–O(2)	2.025(4)
Ru(1)–O(3)	2.064(4)	Ru(1)–N(1)	2.048(4)
Ru(1)–N(2)	1.952(5)	Ru(1)–N(3)	2.064(4)
O(1)–C(1)	1.333(6)	O(2)–C(6)	1.334(6)
O(3)–C(22)	1.246(7)	O(4)–C(22)	1.252(7)
O(4)–O(6)	2.733(7)	O(3)–O(5)	2.990(6)
	Bond Angles (deg)		
O(1)–Ru(1)–O(2)	82.1(2)	O(1)–Ru(1)–O(3)	84.4(2)
O(1)–Ru(1)–O(4)	122.7(1)	O(1)–Ru(1)–N(1)	100.9(2)
O(1)–Ru(1)–N(2)	176.1(2)	O(1)–Ru(1)–N(3)	100.8(2)
O(2)–Ru(1)–O(3)	166.5(2)	O(2)–Ru(1)–O(4)	150.8(1)
O(2)–Ru(1)–N(1)	91.5(2)	O(2)–Ru(1)–N(2)	94.0(2)
O(2)–Ru(1)–N(3)	91.6(2)	O(3)–Ru(1)–O(4)	41.6(1)
O(3)–Ru(1)–N(1)	91.4(2)	O(3)–Ru(1)–N(2)	99.4(2)
O(3)–Ru(1)–N(3)	90.6(2)	O(4)–Ru(1)–N(1)	70.2(2)
O(4)–Ru(1)–N(2)	61.0(2)	O(4)–Ru(1)–N(3)	97.7(2)
O(4)–Ru(1)–H(5)	89(1)	O(4)–Ru(1)–H(15)	115(1)
N(1)–Ru(1)–N(2)	79.1(2)	N(1)–Ru(1)–N(3)	158.3(2)
N(2)–Ru(1)–N(3)	79.3(2)	Ru(1)–O(1)–C(1)	111.3(3)
Ru(1)–O(2)–C(6)	110.9(4)	Ru(1)–O(3)–C(22)	127.3(4)

respectively. The contribution of $[Ru^{I}Cl(qui)(terpy)]$ in the equilibrium can be neglected because of the unusual Ru(I) oxidation state. Since the structure of dioxolene ligand reflects their oxidation state, we examined the bond lengths of dioxolene ligand in complexes **1** and **3**. Semiquinone and quinone ligands usually have two short C–C bonds in the C_6 ring,[8a,10a] while the catechol one does not show a large deviation in C–C bond distances in the ring.[18] The C–O bond lengths of catechol and semiquinone ligands generally have values around 1.35 and 1.29 Å, respectively.

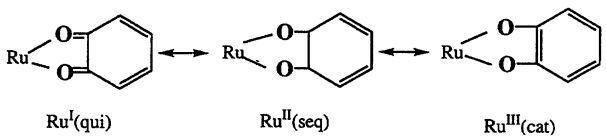

$Ru^{I}(qui)$ $Ru^{II}(seq)$ $Ru^{III}(cat)$

(1)

The $O_2C_6H_2Bu_2$ ligand linked to Ru(1) seems to contain two short C3–C4 (1.32(3) Å) and C5–C6 (1.35(3) Å) bonds, and four long C2–C3, C4–C5, C1–C2 (1.41(3) Å) and C1–C6 (1.44(2) Å) ones in the C_6 ring. Another ligand attached to Ru(2) appears to have one short C34–C35 (1.31(3) Å) and five long C–C bonds (1.40(3)—1.46(3) Å) in the ring. However, the errors of bond lengths are too large to distinguish the coordination modes of two $O_2C_6H_2Bu_2$ ligands bonded to Ru(1) and Ru(2) in **1**. The rather long C–O bond lengths (1.26—1.33 Å) suggest that dioxolene ligands in **1** are in a catechol or in a semiquinone form. On the other hand, the molecular structure of **3** was determined more accurately. Two C–O bond lengths in **3** are 1.333(6) and 1.334(6) Å, and C–C bonds are in the region of 1.37 to 1.41 Å. They are typical lengths in catechol form. The electronic configuration of **3**, therefore, is formulated as a Ru^{III}(catechol) complex.

Redox Behavior and Electronic Absorption Spectra. It has been reported that bis-bipyridine ruthenium complex, $[Ru(bpy)_2(dbcat)]$ undergoes four redox reactions of the (bpy/bpy$^-$), (dbcat/dbseq), (dbseq/dbqui) and (Ru(III)/Ru(II)) couples at $E_{1/2}=-1.99$, -0.75, $+0.15$, and $+1.25$ V vs. SCE ($E_{1/2}=(E_{pc}+E_{pa})/2$) in 1,2-dichloroethane (Scheme 1).[4,11bc] Among these oxidation states of the complex, $[Ru^{II}(dbseq)(bpy)_2]^+$ and $[Ru^{II}(dbqui)(bpy)_2]^{2+}$ are reported to have characteristic strong MLCT bands at 848 and 668 nm, respectively.[4,11bc] The cyclic voltammogram (CV) of **1** in CH_3CN also shows four redox couples at $E_{1/2}=-2.20$, -1.07, -0.23 and $+0.77$ V (vs. Fc/Fc$^+$) with the peak separations ($|E_{pc}-E_{pa}|$) of 130, 60, 60, and 120 mV, respectively (Fig. 4). Based on the rest potential (-0.39 V) of **1** in CH_3CN, the four redox reactions are responsible for the ($\mathbf{1}^{2-}/\mathbf{1}^-$), ($\mathbf{1}^-/\mathbf{1}$), ($\mathbf{1}/\mathbf{1}^+$), and ($\mathbf{1}^+/\mathbf{1}^{2+}$) couples, respectively. Both the ($\mathbf{1}^-/\mathbf{1}$) and ($\mathbf{1}/\mathbf{1}^+$) redox reactions are electrochemically reversible (Fig. 4b) but the ($\mathbf{1}^{2-}/\mathbf{1}^-$) and ($\mathbf{1}^+/\mathbf{1}^{2+}$) redox reactions are followed by chemical reactions giving rise to new anodic waves at -0.85 and -0.02 V. The electronic states of $\mathbf{1}^{2-}$ and $\mathbf{1}^{2+}$ are straightforwardly assigned to $[Ru^{II}Cl(dbcat)(terpy^-)]^{2-}$ and $[Ru^{III}Cl(dbqui)(terpy)]^{2+}$, respectively. The ($\mathbf{1}^{2-}/\mathbf{1}^-$) and ($\mathbf{1}^+/\mathbf{1}^{2+}$) redox reactions, therefore, are responsible for the $[Ru^{II}Cl(dbcat)(terpy^-)]^{2-}/[Ru^{II}Cl(dbcat)(terpy)]^-$ and $[Ru^{II}Cl(dbqui)(terpy)]^+/[Ru^{III}Cl(dbqui)(terpy)]^{2+}$ couples, respectively (Scheme 2). The CV of **1** in CH_2Cl_2 displayed three redox couples at $E_{1/2}=-1.26$, -0.37, and 0.84 V. These redox couples are assigned to ($\mathbf{1}^-/\mathbf{1}$), ($\mathbf{1}/\mathbf{1}^+$),

$[Ru^{II}(dbcat)(bpy^-)(bpy)]^-$ $\rightleftharpoons$ $[Ru^{II}(dbcat)(bpy)_2]$ $\rightleftharpoons$

-1.99 V -0.75 V

$[Ru^{II}(dbseq)(bpy)_2]^+$ $\rightleftharpoons$ $[Ru^{II}(dbqui)(bpy)_2]^{2+}$

+0.15 V

$\rightleftharpoons$ $[Ru^{III}(dbqui)(bpy)_2]^{3+}$

+1.25 V

Scheme 1.

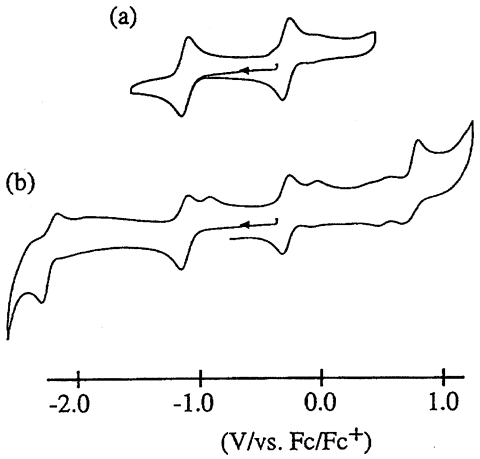

Fig. 4. Cyclic voltammogram of [RuCl(dbcat)(terpy)] in CH_3CN under N_2 atmosphere. $(n\text{-Bu})_4NBF_4$ was used as electrolyte. Scan rate is 1×10^2 mV s^{-1}.

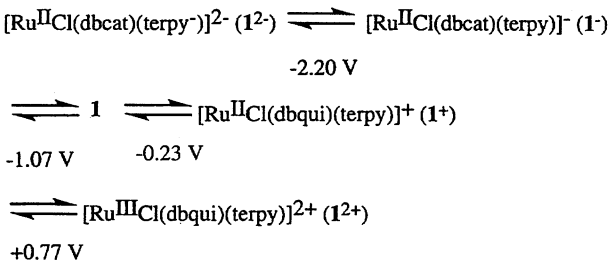

Scheme 2.

and ($\mathbf{1}^+/\mathbf{1}^{2+}$) couples, respectively, judging from the rest potential of −0.47 V of **1** in the same solvent. The remaining ($\mathbf{1}^{2-}/\mathbf{1}^-$) redox couple is probably obscured by strong cathodic currents due to oxidative decomposition of CH_2Cl_2 near −2.0 V region. Though these three redox reactions of **1** in CH_2Cl_2 were already measured,[16] they were related to the ($\mathbf{1}^{2-}/\mathbf{1}^-$), ($\mathbf{1}^-/\mathbf{1}$), and ($\mathbf{1}/\mathbf{1}^+$) redox couples, respectively. The disagreement apparently results from erroneous assignments of the redox couples in CH_2Cl_2 and the rest potential of **1**.

The electronic absorption spectra of **1** and $\mathbf{1}^+$ exhibited strong absorption band at 878 and 600 nm in CH_2Cl_2, respectively. Indeed, the electrochemical oxidation of **1** at 0.22 V (vs. Fc/Fc^+) in CH_2Cl_2 brings about the appearance of the 600 nm band of $\mathbf{1}^+$ at the expense of the 878 nm band of **1** (Fig. 5a). The electrochemical reduction of **1** at −1.48 V in CH_2Cl_2 resulted in disappearance of the strong 878 nm band and appearance of two new weak bands at 428 and 602 nm (Fig. 5b). The oxidation of the resultant solution at −0.7 V regenerated the electronic absorption spectrum of **1**, indicating that $\mathbf{1}^-$ is also a chemically stable species. Based on these electronic absorption spectra,[11b] the electronic configurations of $\mathbf{1}^-$, **1**, and $\mathbf{1}^+$ are reasonably expressed by $[Ru^{II}Cl(dbcat)(terpy)]^-$, $[Ru^{II}Cl(dbseq)(terpy)]$, and $[Ru^{II}Cl(dbqui)(terpy)]^+$, respectively.

The measurement of CV of **2** in CH_3CN was interfered with by substitution reactions of the acetato ligand by the solvent molecule. The redox behavior of **2** in CH_2Cl_2 was

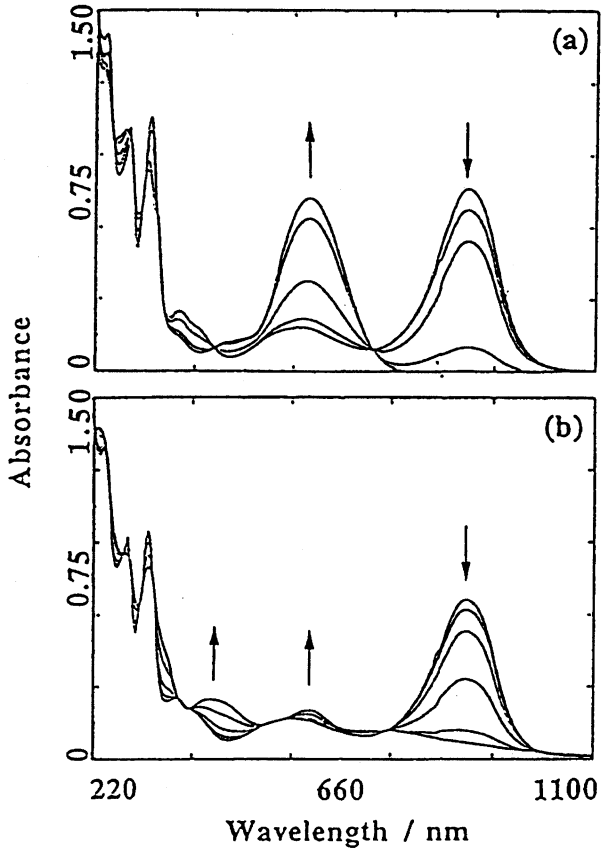

Fig. 5. Spectroelectrochemical UV-vis-near IR spectral change of [RuCl(dbcat)(terpy)] (6.74×10^{-4} mol dm^{-3}) in dichloromethane in an atmosphere of nitrogen under controlled potential electrolyses at 0.22 V (a) and −1.48 V (b) vs. Fc/Fc^+. The optical path length of the cell is 0.5 mm.

quite similar to that of **1** in the same solvent. Three redox reactions of the ($\mathbf{2}^-/\mathbf{2}$), ($\mathbf{2}/\mathbf{2}^+$) and ($\mathbf{2}^+/\mathbf{2}^{2+}$) couples were observed at $E_{1/2}=-1.24$, −0.38, and +0.82 V, respectively, in the CV (Table 6). One-electron reduction and oxidation processes of **3**—**5** were observed in the potential ranges of $E_{1/2}=-1.07$ to −0.78 and −0.21 to 0.18 V, respectively. The ($\mathbf{1}/\mathbf{1}^+$) and ($\mathbf{2}/\mathbf{2}^+$) redox couples were observed at $E_{1/2}=$ +0.84 and +0.82 V, though those of **3**—**5** were not detected in CH_2Cl_2 due to the irreversible oxidation of the solvent

Table 6. Electrochemical Parameters for Ruthenium–terpyridine– dioxolene Complexes, [RuL(dioxolene)-(terpy)]X

			$E_{1/2}$[a]/V vs. Fc/Fc^+(ΔE/mV)		
Complex	Dioxolene	L	−1/0	0/+1	+1/+2
1	dbcat	Cl	−1.26(118)	−0.37(110)	0.84(142)
2	dbcat	OAc	−1.24(150)	−0.38(150)	0.82[b]
3	cat	OAc	−1.07(157)	−0.21(170)	
4	Cl_4-cat	OAc	−0.80(150)	0.19(150)	
5	NO_2-cat	OAc	−0.78(140)	0.18(140)	

a) $E_{1/2}=1/2(E_{pa}-E_{pc})$. $\Delta E=E_{pa}-E_{pc}$. Scan rate is 1×10^2 mV s^{-1}. Measured in dichloromethane containing $(n\text{-Bu})_4NBF_4$ (0.1 M) as a supporting electrolyte. b) Irreversible.

at potentials more positive than 1.0 V. The $E_{1/2}$ values of the one-electron reduction and oxidation of the acetato complexes (**2**—**5**) are largely influenced by the substituents of the dioxolene ligand, and shifted to positive potentials in the order of **2**<**3**<**4**≈**5**. This result indicates that these redox reactions primarily take place at dioxolene moieties rather than at Ru.

IR Spectra. From the viewpoint of the strong electronic absorption bands around 800 and 600 nm of the neutral complexes **1**—**5** and the cationic complexes $\mathbf{1}^+$—$\mathbf{3}^+$,respectively, the electronic states of these complexes are formulated as [Ru^{II}Cl(seq)(terpy)] and [Ru^{II}Cl(qui)(terpy)]$^+$ (vide supra). We also measured the IR spectra to examine the charge distribution in ruthenium dioxolene complex. The binding modes of dioxolene ligands are tentatively distinguished from their ν(CO) bands;[6,11] for catecholato complexes ν(C–O) is observed at around 1200 cm^{-1}, for semiquinone complexes ν(C–O) band is in the ranges of 1400—1500 cm^{-1}, and for quinone complexes, ν(C=O) appears at around 1600 cm^{-1}.[19] Figure 6 shows the IR spectra of **1**and **1**·BF_4. The most distinct difference between the two IR spectra is that the spectrum of **1** shows a very strong absorption band at 1194 cm^{-1}, which completely disappears in the IR spectrum of $\mathbf{1}^+$ around 1200 cm^{-1}. The 1194 cm^{-1} band of **1** is assigned to the ν(C–O) band of catecholato moiety, while a ν(C–O) band associated with semiquinone group was not identified in the IR spectra of **1**. A strong band at 1601 cm^{-1} with a shoulder at 1591 cm^{-1} of $\mathbf{1}^+$ is related to the ν(C=O) band of the quinone moiety even though **1** displays two weak bands at 1599 and 1581 cm^{-1}. Thus, the electronic state of **1** is represented by [Ru^{III}(terpy)(dbcat)Cl] rather than [Ru^{II}Cl(dbseq)(terpy)] on the basis of the IR spectra. Furthermore, **2** and **3** showed a strong ν(C–O) band at 1198 at 1240 cm^{-1} respectively, which disappeared upon the one-electron oxidation of the complexes. The resultant $\mathbf{2}^+$ and $\mathbf{3}^+$ displayed the ν(C=O) band at 1603 and 1605 cm^{-1}, respectively. It is worthy to note that **4** and **5**, which were not oxidized by Ag^+, also exhibited a strong ν(C–O) band at 1240 and 1256 cm^{-1}, respectively. Based on these IR spectra, the electronic states of [Ru^{III}(terpy)(cat)X] and [Ru^{II}(terpy)(qui)X]$^+$ reasonably account for the strong bands in the range of 1194 to 1256 cm^{-1} of the neutral complexes **1**—**5** and for those around 1600 cm^{-1} of mono-cationic species $\mathbf{1}^+$—$\mathbf{3}^+$.

ESR Spectra. From the preceding discussions, the electronic configurations of cationic $\mathbf{1}^+$, $\mathbf{2}^+$, and $\mathbf{3}^+$ are reasonably represented by Ru^{II}–quinone. On the other hand, coordination modes of dioxolene ligands to Ru in neutral complexes, **1**—**5**, are not consistent with each other based on the criteria reported so far;[4,8,11,18,19] Ru^{III}(catecol) is indicated by X-ray and IR spectra, while the electronic spectra and cyclic voltammetry of the complexes are interpreted as the electronic structure of a Ru^{II}(semiquinone) complex. ESR would give more direct information about the electronic structures between Ru^{III}(catecol) and Ru^{II}(semiquinone) by assuming that the unpaired electron residing in Ru^{III} and semiquinone displays an anisotropic and a relatively sharp isotropic signal, respectively. The electronic structure of **1** has been assigned to a Ru^{II}(dbseq) complex on the basis of the ESR spectra of an apperance of a slightly anisotropic pattern on a broad isotropic signal at 77 K and a broad isotropic signal (g≈2.0) at 298 K. On the other hand, the ESR spectrum of [Ru(OAc)-(Cl_4cat)(terpy)] (**4**) in dichloromethane at 5 K (Fig. 7a) is composed of an axial pattern consisting of g_1=2.27, g_2=2.13, and g_3=2.00, derived from a large contribution of the Ru(III)

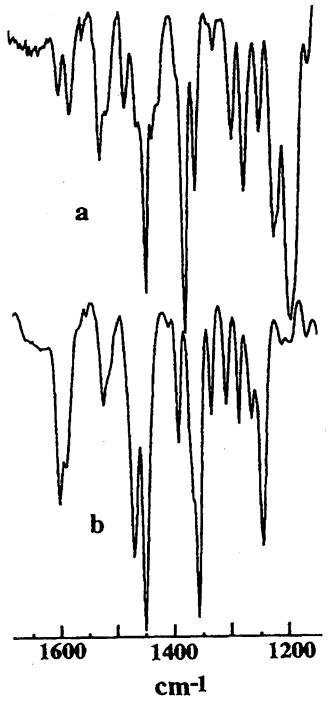

Fig. 6. IR spectra of [RuCl(dbcat)(terpy)] (a) and [RuCl-(dbcat)(terpy)]BF_4 (b) in KBr pellet.

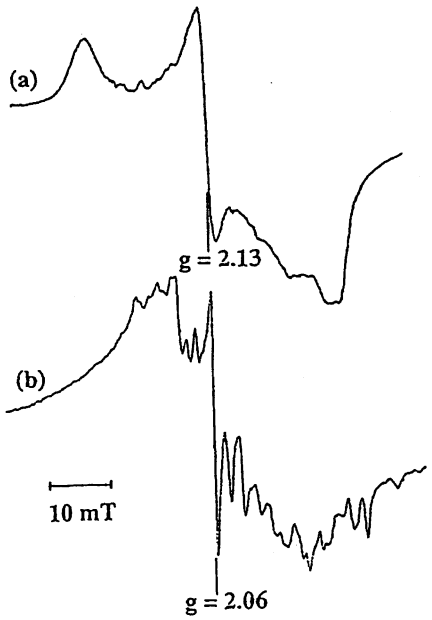

Fig. 7. ESR spectra of [Ru(OAc)(Cl_4-cat)(terpy)] at 5 K (a) and [Ru(OAc)(cat)(terpy)] at 77 K (b) in dichloromethane under reduced pressure.

center with a d^5 low spin population.[11,20] The axial pattern disappeared at 77 K to afford only an isotropic broad signal at g=2.08 with a half-height-width of 20.5 mT. Furthermore, the ESR spectrum of [Ru(OAc)(cat)(terpy)] (**3**) at 77 K exhibited hyper-fine structures superimposed upon an axial pattern of the Ru(III) center (Fig. 7b). The hyper-fine structures of **3** were observed between 10 and 140 K, and became an isotropic broad signal at g=2.06 with a half-width of 21.5 mT above 140 K. The broad signal decreased in intensity as temperature was further raised and almost disappeared at 260 K. The spectrum of **5** also was composed of complicated hyper-fine lines superimposed upon an axial pattern as similar to that of Fig. 7b. Thus, the ESR spectra of **4** at 5K (Fig. 7a) is responsible for the electronic structure of a Ru^{III}(catechol) complex, while the appearance of the hyper-fine structures in the anisotropic signal (Fig. 7b) is explained by the large contribution of the Ru^{II}(semiquinone) form.[21] Thus, the energy difference between [Ru^{II}X(semiquinone)-(terpy)] and [Ru^{III}X(catecholato)(terpy)] is not large enough to distinguish the two states. The fact, however, that the Ru(dioxolene) complexes with a good leaving group stably undergo one-electron reduction and oxidation reactions without accompanying serious configurational changes indicates the potentiality as two electron resirvors in electrocatalysts which can operate at potentials more positive than the redox potentials of Ru(polypyridyl) complexes.

References

1) a) J. Costamagna, G. Ferraudi, J. Canales, and J. Vargas, *Coord. Chem. Rev.*, **148**, 221 (1996); b) H. Nagao, T. Mizukawa, and K. Tanaka, *Inorg. Chem.*, **33**, 3415 (1994); c) K. Toyohara, H. Nagao, T. Mizukawa, and K. Tanaka, *Inorg. Chem.*, **34**, 5399 (1995).

2) H. Nakajima, Y. Kushi, H. Nagao, and K. Tanaka, *Organometallics*, **14**, 5093 (1995).

3) H. Nakajima, H. Nagao, and K. Tanaka, *J. Chem. Soc., Dalton Trans.*, **1996**, 1405.

4) M. Haga, K. Isobe, S. R. Boone, and C. G. Pierpont, *Inorg. Chem.*, **29**, 3795 (1990).

5) a) D. J. Gordon, and R. F. Fenske, *Inorg. Chem.*, **21**, 2907 (1982); b) D. J. Gordon and R. F. Fenske, *Inorg. Chem.*, **21**, 2916 (1982).

6) a) C. G. Pierpont and C. W. Lange, *Prog. Inorg. Chem.*, **41**, 331 (1994); b) C. G. Pierpont and R. M. Buchanan, *Coord. Chem. Rev.*, **38**, 45 (1981).

7) C. G. Pierpont and R. M. Buchanan, *J. Am. Chem. Soc.*, **97**, 4912 (1975).

8) a) S. R. Boone, G. H. Purser, H.-R. Chang, M. D. Lowery, D. N. Hendrickson, and C. G. Pierpont, *J. Am. Chem. Soc.*, **111**, 2292 (1989); b) D. Zirong, S. Bhattacharya, J. K. McCusker, P. M. Hagen, D. N. Hendrickson, and C. G. Pierpont, *Inorg. Chem.*, **31**, 870 (1992); c) S. A. Attia, B. J. Conklin, C. W. Lange, and C. G. Pierpont, *Inorg. Chem.*, **35**, 1033 (1996).

9) a) R. M. Buchanan, C. W.-Blumenberg, C. Trapp, S. K. Larsen, D. L. Greene, and C. G. Pierpont, *Inorg. Chem.*, **25**, 3070 (1986); b) S. Bhattacharya, S. R. Boone, G. A. Fox, and C. G. Pierpont, *J. Am. Chem. Soc.*, **112**, 1088 (1990).

10) a) R. M. Buchanan and C. G. Pierpont, *J. Am. Chem. Soc.*, **102**, 4951 (1980); b) O. -S. Jung and C. G. Pierpont, *Inorg. Chem.*, **33**, 2227 (1994).

11) a) A. B. P. Lever, P. R. Auburn, E. S. Dodsworth, M. Haga, W. Liu, M. Melnik, and A. Nevin, *J. Am. Chem. Soc.*, **110**, 8076 (1998); b) M. Haga, E. S. Dodsworth, and A. B. P. Lever, *Inorg. Chem.*, **25**, 447 (1986); c) H. Masui, A. B. P. Lever, and P. R. Auburn, *Inorg. Chem.*, **30**, 2402 (1991); d) C. J. da Cunha, S. S. Fielder, D. V. Stynes, H. Masui, P. R. Auburn, and A. B. P. Lever, *Inorg. Chem. Acta*, **242**, 293 (1996).

12) S. Bhattacharya and C. G. Pirepont, *Inorg. Chem.*, **31**, 35 (1992).

13) R. A. Leising, S. A. Kubow, M. R. Churchill, L. A. Buttrey, J. W. Ziller, and K. J. Takeuchi, *Inorg. Chem.*, **29**, 1306 (1990).

14) "TEXSAN: Single Crystal Structure Analysis Software," Version 1.6, Molecular Structure Corp., The Woodlands, TX 77381 (1993).

15) "MULTAN88: Computer Programs for the Automatic Solution of Crystal Structures from X-Ray Diffraction Data," ed by T. Debaerdemeaker, G. Germain, P. Main, L. S. Refaat, C. Tate, and M. M. Woolfson, University of York, U. K. (1988).

16) S. Bhattacharya, *Polyhedron*, **13**, 451 (1994).

17) S. R. Boone and C. G. Pierpont, *Polyhedron*, **9**, 2267 (1990).

18) a) J. R. Hartman, B. M. Foxman, and S. R. Cooper, *Inorg. Chem.*, **23**, 1381 (1984); b) P. B. Kettler, Y.-D. Chang, J. Zubieta, and M. J. Abrams, *Inorg. Chim. Acta*, **218**, 157 (1994).

19) S. D. Pell, R. B. Salmonsen, A. Abelleira, and M. J. Clarke, *Inorg. Chem.*, **23**, 385 (1984).

20) a) N. Bag, A. Pramanik, G. K. Lahiri, and A. Chakravorty, *Inorg. Chem.*, **31**, 40 (1992); b) P. T. Manoharan, P. K. Mehrotra, M. M. Taguikhan, and R. K. Andal, *Inorg. Chem.*, **12**, 2753 (1973); c) O. K. Medhi and U. Agarwala, *Inorg. Chem.*, **19**, 1381 (1980).

21) a) M. E. Cass, D. L. Greene, R. M. Buchanan, and C. G. Pierpont, *J. Am. Chem. Soc.*, **105**, 2680 (1983); b) L. I. Simándi, T. Barna, G. Argay, and T. L. Simándi, *Inorg. Chem.*, **34**, 6337 (1995); c) F. Hartl and A. Vlcek, Jr., *Inorg. Chem.*, **35**, 1257 (1996); d) M. A. Brown, B. R. McGarvey, A. Ozarowski, and D. G. Tuck, *Inorg. Chem.*, **35**, 1560 (1996).